

**Solomon C. Yim**  
Professor  
Fellow ASME

**Dongjun Yuk**  
Post-Doctoral Fellow

Department of Civil Engineering,  
Oregon State University,  
Corvallis, OR 97331-2302

**Arvid Naess**  
Professor  
Fellow ASME

Department of Mathematical Science,  
Norwegian University of Science and Technology,  
NO-7491, Trondheim, Norway

**I-Ming Shih**  
Former Graduate Student

Department of Civil Engineering,  
Oregon State University,  
Corvallis, OR 97331-2302

# Stochastic Analysis of Nonlinear Responses of a Moored Structure Under Narrow Band Excitations

*A semianalytical method is developed for the stochastic analysis of a nonlinear moored ocean structure subjected to narrow band random waves. The method is then used to investigate the probability distribution of extreme values of the responses. To verify the accuracy and capability of the method in handling complex nonlinear behavior of the nonlinear moored ocean structure, experimental results are employed to calibrate numerical simulations and the resulting probability distributions obtained from the semianalytical method. A nonlinear-structure nonlinearly damped model is employed to model the moored structure considered and the system coefficients are identified through the reverse multiple-input/single-output technique. An examination of the comparisons indicates that the structural response extreme value probability distributions obtained from the semianalytical predictions are quite accurate. [DOI: 10.1115/1.2827878]*

## Introduction

Nonlinear dynamic behaviors of ocean structures have been studied for decades [1–6]. It is well known that nonlinear system responses can exhibit very complex behaviors such as coexisting attraction domains, instability, jump phenomena, and chaos [3,4,7]. Such typical nonlinear response behaviors have been observed for moored ocean structures subjected to random ocean waves [8,9]. To analyze the nonlinear response behaviors of moored ocean structures, a semianalytical method is developed in this study, in which the moored ocean structure is modeled by the Duffing equation containing cubic nonlinear restoring force terms [7]. In the equation, the structural dynamic damping is approximated by a linearized damping term. In a recent study [10,11], it is shown that the moored system under narrow band excitation can be most accurately described by a nonlinear-structure nonlinearly damped (NSND) model (among several different models considered). In the NSND model, the hydrodynamic drag and inertia forces are considered in addition to the hydrodynamic damping force.

## System Description

An experiment was performed at the O. H. Hinsdale Wave Research Laboratory at Oregon State University on a multipoint moored submerged sphere under wave excitation [12]. The experimental model consists of a spherical rigid body of 0.46 m diameter with a 0.0254 m<sup>2</sup> rectangular shaped rod through the center supported by guyed masts 1.83 m above the bottom of a wave channel. The system behaves as a single-degree-of-freedom with the motion of the sphere constrained to the surge direction only. The sphere, made of PVC, is filled with water when submerged. Springs are attached to the sphere to provide a nonlinear restoring force (see Fig. 1).

Steady-state system responses under deterministic wave excitations over a wide range of wave frequencies are examined first. Periodic wave excitations with sufficiently long duration are applied to the moored structure to achieve steady-state responses. Superharmonic, primary, and subharmonic resonance responses are observed around regions with wave frequency centralized at 0.14 Hz, 0.27 Hz, and 0.50 Hz, respectively (Fig. 2, [8,9]). Notice that while the primary resonance is clearly demonstrated, the superharmonic and subharmonic resonance regions are indicated by the smaller maxima. In the subharmonic resonance region, the sphere oscillates at a frequency near one-half that of the excitation, indicating the responses are 1/2 subharmonics. Dashed lines in the figure show the estimated stability boundaries of the corresponding superharmonic, primary, and subharmonic resonance regions.

In this study, we are interested in examining the transition behaviors between 1/2 subharmonic and harmonic system responses. For this purpose, narrow band random excitations with dominant frequencies centered at 0.5 Hz (the subharmonic resonance region) will be employed. Corresponding experimental tests of the moored ocean system will also be examined and used to calibrate analytical predictions and simulation results.

## Equation of Motion

The general form of the equation of motion can be written as

$$m\ddot{x}(t) + C_s\dot{x}(t) + R(x(t)) = f(t) \quad (1)$$

where  $m$  = mass,  $C_s$  = damping coefficient,  $R(x(t))$  = restoring force, and  $f(t)$  = forcing. For the modeling of the moored sphere, hydrodynamic inertia and drag force are considered. The nonlinear equation of motion for the NSND model is given by [10]

$$(m + m_d)\ddot{x}(t) + C_s\dot{x}(t) + a_1x(t) + a_2x^2(t) + a_3x^3(t) + \rho C_d' \frac{\pi}{4} D^2 \dot{x}(t) |\dot{x}(t)| = f(t) \quad (2)$$

where

Contributed by the Ocean Offshore and Arctic Engineering Division of ASME for publication in the JOURNAL OF OFFSHORE MECHANICS AND ARCTIC ENGINEERING. Manuscript received December 29, 2005; final manuscript received November 9, 2007; published online January 29, 2008. Review conducted by Antonio C. Fernandes.

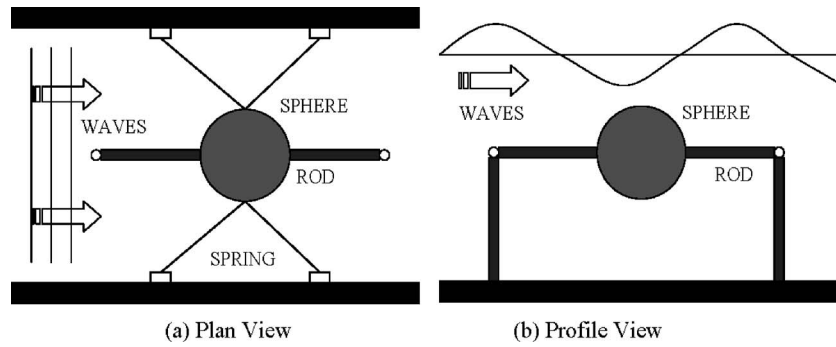


**Fig. 1 Experimental model of a submerged, hydrodynamically damped, and excited structural system**

$$f(t) = \rho \frac{\pi}{6} D^3 C_m \dot{u}(t) + \rho C_d \frac{\pi}{4} D^2 u(t) |u(t)|$$

$$u(t) = a\omega \frac{\cosh(ks)}{\sinh(kh)} \cos(kx(t) - \omega t)$$

$m_a$ =added mass,  $C_d$ =hydrodynamic drag coefficient,  $C_m$ =hydrodynamic inertia coefficient,  $C_s$ =linear damping coefficient,  $C'_d$ =nonlinear structural damping coefficient,  $\rho$ =water density, and  $D$ =diameter of the sphere. Linear wave theory is used to characterize the horizontal water particle velocity,  $u(t)$ . For the rigid body free to move in waves, an independent flow-field model is used as an alternating form for the Morison equation [10,13]. In this study, the linear superposition of two independent flow fields separating the wave motion and the motion of the structure is used. For accurate modeling of the structural system considered by NSND model, the coefficients of the governing equation of motion should be determined accurately. A system identification technique developed in a previous study by Narayanan and Yim [10] is used to determine the coefficients. It is shown that the system response with the coefficients determined by the system identification technique matches the experimental results accurately.

### Amplitude Jump Phenomena

A typical nonlinear response behavior, the amplitude jump [7], which is observed in both analytical predictions and experiments, can be characterized by the response amplitude curve. The amplitude jumps occur when the excitation amplitude gradually drifts out of attraction domain boundaries. This jump phenomenon is defined as an interdomain transition. For the specific set of system parameters,  $m=3.428$ ,  $C_a=0.25$ ,  $\xi=0.06$ ,  $C'_d=0.02$ ,  $C_m=1.25$ ,  $C_d$

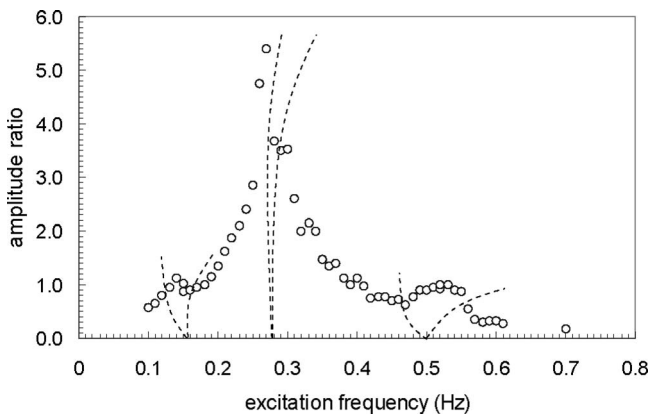


**Fig. 2 Frequency response diagram (experimental results); (---) estimated stability boundaries**

$=0.1$ ,  $a_1=9.3$ ,  $a_2=4.0$ ,  $a_3=4.0$ , three different attraction domains are found over the region of excitation amplitudes and frequencies considered. The nonlinear system response dependency on initial conditions is shown in Fig. 3. For trajectories with initial displacements and velocities highlighted in Fig. 3(a), the steady-state responses result in a 1/2 subharmonic. On the other hand, when the initial conditions belong to the regions highlighted in Fig. 3(b), the resulting steady-state responses are large amplitude harmonics. The time series shown in Fig. 4 demonstrates the amplitude jump phenomenon from the small amplitude harmonic attraction domain to the large amplitude harmonic domain when excitation amplitudes increased from 0.750 to 0.753. The system initially is subjected to deterministic excitation with amplitude  $A=0.750$  until the peak-to-trough system response stabilizes at 0.76. The “steady-state” response shows the small amplitude harmonic response having the same frequency as the excitation. Then, the excitation amplitude is increased from  $A=0.750$  to  $A=0.753$  at time=600 s. For such a small increase in amplitude, it is observed that the steady-state peak-to-trough response is increased to 1.72, a more than twice increase in magnitude.

The response amplitude curves shown in Fig. 5 are the steady-state response amplitudes under deterministic excitation obtained by numerical integration of the equation of motion. As shown in the figure, transitions among different domains depend on the attraction domains that the system response belongs to at the moment of excitation variation and the direction of excitation amplitude change (i.e., increase or decrease). For example, as the excitation amplitude slowly decreases from  $A_{2U} < A < A_{1U}$  to  $A_{2L} < A < A_{2U}$ , the occurrence of jump phenomenon depends on the current attraction domain the response belongs to. If the system response belongs to the large amplitude domain ( $D_3$ ), amplitude jump will not occur. However, when the small amplitude domain ( $D_1$ ) is the current attraction domain, transition from  $D_1$  to 1/2 subharmonic domain ( $D_2$ ) will occur. With infinitesimal variations in excitation amplitude, jumps from  $D_3$  to  $D_1$ , and from  $D_3$  to  $D_2$  cannot occur. For the gradual excitation amplitude variation within an attraction domain, response amplitude varies along the response amplitude curve. When the excitation amplitudes are increased from 0 to beyond the small amplitude harmonic domain upper boundary  $A_{1U}$ , transitions occur from  $D_1$  to  $D_2$  and  $D_2$  to  $D_1$  and  $D_1$  to  $D_3$ . On the other hand, for the excitation amplitude decreasing from  $A > A_{1U}$  to 0, responses undergo the transitions from  $D_3$  to  $D_2$  and  $D_2$  to  $D_1$ . All possible transitions and variations of system response amplitudes with increasing and decreasing (deterministic) harmonic excitation amplitudes in the given range are shown in the figure.

For stochastic excitation model with the finite variation in excitation amplitude, response amplitude curves become response amplitude map where groups of data points indicating existence of corresponding attraction domains [9]. Notice that transitions from  $D_3$  to  $D_1$  and  $D_2$  to  $D_3$  are assumed to occur even though the

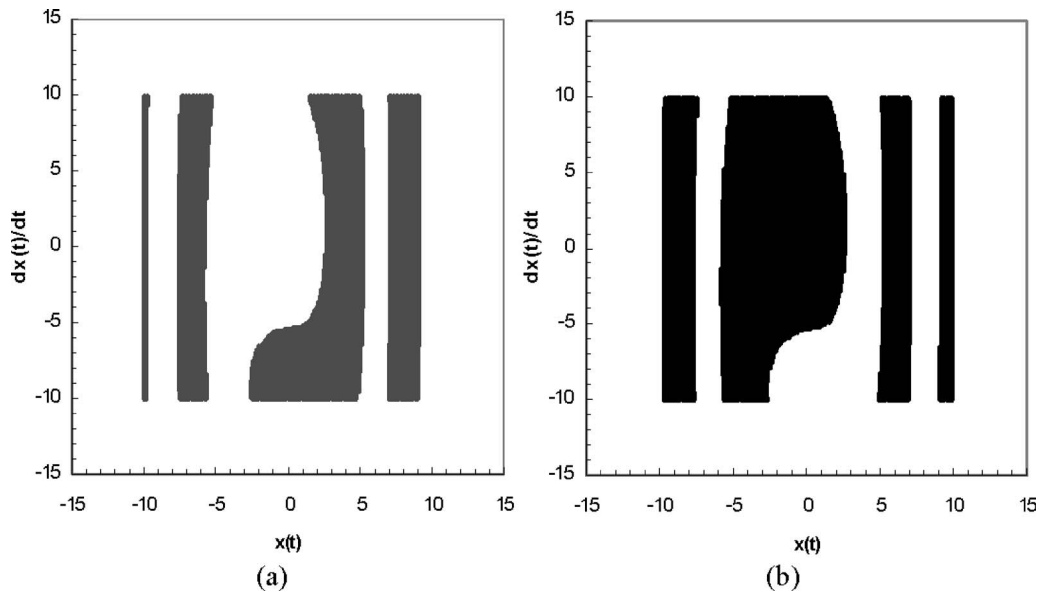


Fig. 3 Coexisting attraction domain (a) 1/2 subharmonic attraction domain; (b) large harmonic attraction domain {A=1.0}

occurrences of those transitions are highly unlikely. The dashed lines in Fig. 5 indicate the transitions considered to occur with finite excitation amplitude variations.

### Stochastic Excitation Parameters

Assuming that the excitation is a Gaussian random process with a narrow band spectrum, the excitation force,  $f(t)$ , can be written as [14]

$$f(t) = A(t)\cos\{\omega_f t + \varepsilon(t)\} \quad (3)$$

The four dimensional joint probability density function of the random variables representing the excitation amplitudes and phase angles corresponding to consecutive excitation cycles, i.e.,  $A(1)$ ,  $A(2)$ ,  $\phi(1)$ , and  $\phi(2)$ , is given by [14]

$$p(A^{(1)}, \phi^{(1)}, A^{(2)}, \phi^{(2)}) = \frac{A^{(1)}A^{(2)}}{4\pi^2\sqrt{|\Sigma|}} \exp\left\{ \frac{-1}{2\sqrt{|\Sigma|}} \left[ \sigma_f^2 [(A^{(1)})^2 + (A^{(2)})^2] - 2A^{(1)}A^{(2)}[\rho \cos(\phi^{(2)} - \phi^{(1)}) + \lambda \sin(\phi^{(2)} - \phi^{(1)})] \right] \right\} \quad (4)$$

where

$$0 \leq A^{(1)}, A^{(2)} < \infty; 0 \leq \phi^{(1)}, \phi^{(2)} \leq 2\pi$$

and

$$\rho = \int_0^\infty S_{ff}(\omega) \cos[(\omega - \omega_f)T] d\omega$$

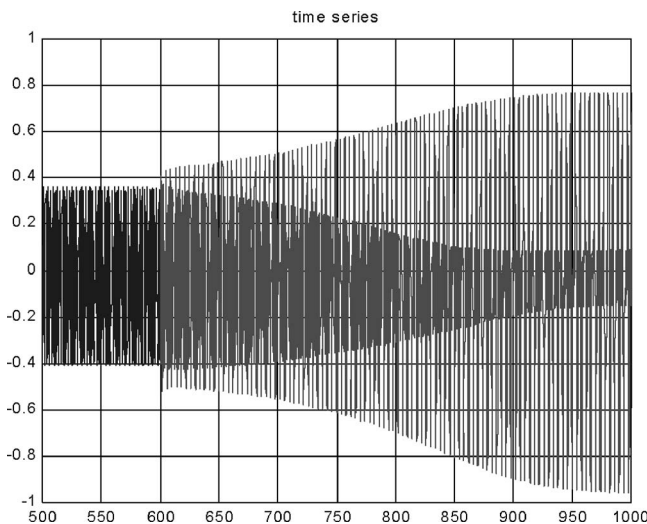


Fig. 4 Time series of the system response under deterministic excitation {A=0.75 for  $t \leq 600$  s, A=0.85 for  $t > 600$  s}

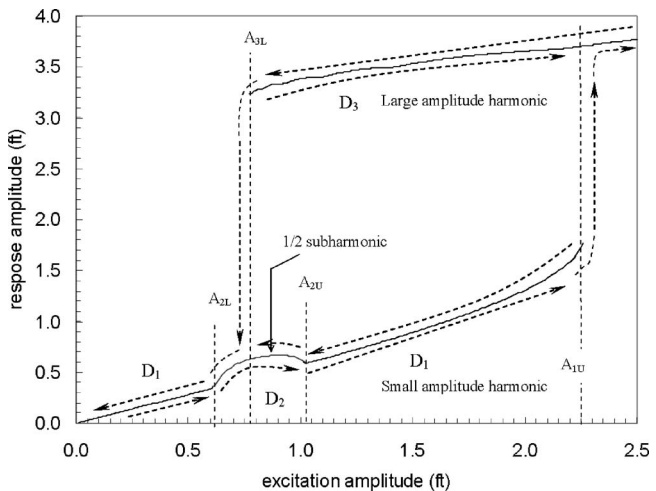


Fig. 5 Response amplitude curve { $m=3.428$ ,  $C_a=0.25$ ,  $\xi=0.06$ ,  $C'_d=0.02$ ,  $C_m=1.25$ ,  $C_d=0.1$ ,  $a_1=9.3$ ,  $a_2=4.0$ ,  $a_3=4.0$ }; transitions and variations of system response amplitude along the response amplitude curves are also shown

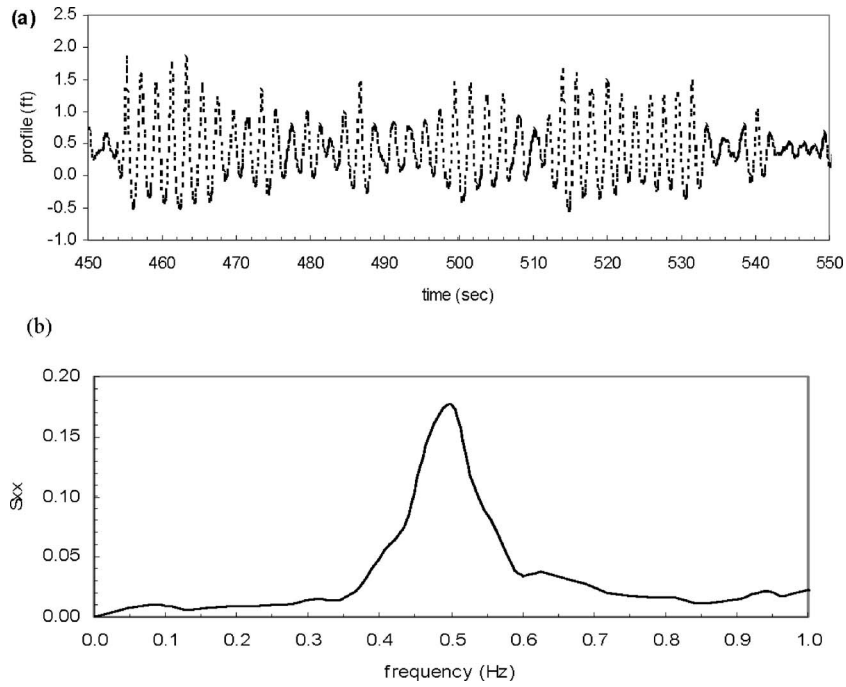


Fig. 6 Experimental excitation: (a) wave profile; (b) wave spectra

$$\lambda = \int_0^{\infty} S_{ff}(\omega) \sin[(\omega - \omega_f)T] d\omega$$

$$\sqrt{|\Sigma|} = \sigma_f^4 - \rho^2 - \lambda^2 \quad (5)$$

and superscripts<sup>1,2</sup> indicate that the quantities are in the current and the next excitation cycles, respectively;  $S_{ff}(\omega)$  is the one-sided spectral density function of  $f(t)$ , and  $T$  is the excitation period equal to  $2\pi/\omega_f$ . The spectral density function of a time series is usually obtained numerically using a standard data analysis procedure. A typical example of the excitation time series and its spectral density are shown in Figs. 6(a) and 6(b), respectively. All stochastic parameters of the excitation random process can be obtained from the spectral density of the time series. If a random variable  $\Phi$  is introduced to represent the phase angle difference  $\phi^{(2)} - \phi^{(1)}$ , the joint PDF of  $A^{(1)}, A^{(2)}$ , and  $\Phi$  can be obtained from Eq. (4) by a transformation of the random variables [14]

$$p(A^{(1)}, A^{(2)}, \Phi) = \frac{A^{(1)}A^{(2)}}{2\pi\sqrt{|\Sigma|}} \exp \left\{ \frac{-1}{2\sqrt{|\Sigma|}} [\sigma_f^2[(A^{(1)})^2 + (A^{(2)})^2] - 2A^{(1)}A^{(2)}[\rho \cos(\Phi) + \lambda \sin(\Phi)]] \right\}$$

$$- 2\pi \leq \Phi \leq 2\pi \quad (6)$$

In addition, the joint PDF of  $A^{(1)}$  and  $A^{(2)}$  can be obtained by integrating Eq. (6) with respect to  $\Phi$  to obtain

$$p(A^{(1)}, A^{(2)}) = \frac{A^{(1)}A^{(2)}}{\sqrt{|\Sigma|}} \exp \left\{ \frac{-1}{2\sqrt{|\Sigma|}} \sigma_f^2 [(A^{(1)})^2 + (A^{(2)})^2] \right\}$$

$$\times I_0 \left( \frac{A^{(1)}A^{(2)}}{\sqrt{|\Sigma|}} \sqrt{\rho^2 + \lambda^2} \right) \quad (7)$$

where  $I_0(x)$  denotes the modified Bessel function of order zero.

### Interdomain Transition

When the stochastic excitation is applied to the system, excitation amplitude, frequency, and phase keep varying from cycle to

cycle. Due to the variation of the excitation parameters, the system response undergoes transition from one attraction domain to another attraction domain. To describe the transition between different attraction domains, a transition probability formulation is employed. The governing equation for interdomain transition is given by

$$\hat{p}(D^{(2)}) = K\hat{p}(D^{(1)}) \quad (8)$$

where  $K$  is the transition matrix whose dimension is  $n \times n$  ( $n$  = the number of coexisting attraction domains = 3), and superscripts (1) and (2) denote the current and next cycles, respectively. The element of the transition matrix  $K$  in  $i$ th row and  $j$ th column is a conditional probability,  $p(i|j)$ , where  $i$  is the attraction domain of the next cycle and  $j$  is the attraction domain of the current cycle. The conditional probabilities can be evaluated by considering the stochastic behavior of the excitation amplitude and system response interdomain transition behavior. For the system response to stay in the same attraction domain,  $D_d$ , in both current and next cycle, the excitation amplitude must remain within same domain,  $D_d^A$ , as in the current cycle. The probability of the excitation amplitude given that it is in the domain,  $D_d^A$ , can be written as

$$p(A|D_d^A) = \frac{p(A)}{\int_{D_d^A} p(A) dA} \quad A \in D_d^A \quad (9)$$

where  $p(A)$  is Rayleigh distribution. Then, the probability distribution of the excitation amplitude in the next cycle given that the excitation amplitude is in  $D_d^A$  in the current cycle can be expressed as

$$p(A^{(2)}|A^{(1)} \in D_d^A) = \int_{D_d^A} p(A^{(2)}|A^{(1)}) p(A^{(1)}|D_d^A) dA^{(1)} \quad (10)$$

Thus, the probability of the system response amplitude remaining in the same attraction domain,  $D_d$ , in the next cycle is

$$P(R^{(2)} \in D_d^R | R^{(1)} \in D_d^R) = \int_{D_d^A} p(A^{(2)} | A^{(1)} \in D_d^A) dA^{(2)} \quad (11)$$

The conditional probability given by Eq. (11) is equal to the diagonal elements of the interdomain transition matrix,  $p(i|i)$ . The off-diagonal elements of  $K$  can be determined by considering the transient-state system mean energy, or equivalently, the transient-state response amplitude.

### Intradomain Transition

The system response undergoes successive transient-state transitions within the attraction domain as the excitation parameter varies within an excitation amplitude domain. These transitions within attraction domains are defined as intradomain transitions. The governing equation of the response amplitude probability intradomain transition can be written as

$$p(R^{(2)} | D_d^R) = \int \left\{ \int \left[ \int p(R^{(2)} | R^{(1)}, A^{(1)}, A^{(2)}, D_d^R) p(R^{(1)} | (D_d^R)_A^{(1)}) dR^{(1)} \right] \times p(A^{(1)} | D_d^A) dA^{(1)} \right\} p(A^{(2)} | D_d^A) dA^{(2)} \quad (12)$$

where

$$p(R^{(2)} | (D_d^R)_A^{(2)}) = \int_{D_d^A} p(R^{(2)} | A^{(1)}, A^{(2)}, D_d^R) p(A^{(1)} | D_d^A) dA^{(1)} \quad (13)$$

and

$$p(R^{(2)} | A^{(1)}, A^{(2)}, D_d^R) = \int_{D_d^A} p(R^{(2)} | A^{(1)}, A^{(2)}, D_d^R) p(R^{(1)} | (D_d^R)_A^{(1)}) dR^{(1)} \quad (14)$$

**Table 1 Parameters of narrowband excitation on SDOF, 90 deg configuration**

Test	D15	D16	D17	D18	D19
System parameters	$C_s=0.76 \ a_1=9.3 \ a_2=4.0 \ a_3=4.0$				
Excitation Parameters in Eq. (5)					
$\omega_f$	$\pi$				
$\sigma_f^2$	0.0675	0.1434	0.2178	0.2210	0.4050
$\rho$	0.0206	0.0344	0.0632	0.0634	0.1236
$\sqrt{ \Sigma }$	0.0041	0.0194	0.0434	0.0448	0.1488

To evaluate the intradomain transition probability, the response amplitude domains  $\{(D_d^R)_A^{(z)}, z=1,2\}$ , the system initial condition  $X_o$  domain, the excitation phase angle difference  $\Phi$  domain, and the excitation amplitude domain  $D_d^A$  are discretized. The initial condition is assumed to be uniformly distributed over the domain (which is the phase trajectory of the current excitation cycle). Then, the first term on the right-hand side of Eq. (14) can be evaluated by the following equation:

$$p(R_k^{(2)} | R_l^{(1)}, A_j^{(1)}, A_i^{(2)}, D_d^R) = p(\Phi_p, X_p^o | R_l^{(1)}, A_j^{(1)}, A_i^{(2)}, D_d^R) = \frac{1}{m_x} \int_{\Phi_p - \Delta\Phi/2}^{\Phi_p + \Delta\Phi/2} \frac{p(A_j^{(1)}, A_i^{(2)}, \Phi)}{p(A_j^{(1)}, A_i^{(2)})} d\Phi \quad (15)$$

where  $m_x$  is the total number of intervals of initial condition  $X_o$  and the subscripts indicate sample points of the corresponding discretized random variables. The probability vector of the response amplitude  $p(R^{(2)} | R_l^{(1)}, A_j^{(1)}, A_i^{(2)}, D_d^R)$  can be obtained by varying  $\Phi_p$  and  $X_p^o$  over the entire respective domains and lumping all  $p(R_k^{(2)} | R_l^{(1)}, A_j^{(1)}, A_i^{(2)}, D_d^R)$ . Then, the discrete form of Eqs. (12)–(14) can be used to determine the intradomain transition probability vectors as follows:

**Table 2 Interdomain transition probability in the subharmonic resonance region**

Test	$\sigma_f^2$	Transition matrix, $K$	Normalized eigenvector
D15	0.0675	$\begin{bmatrix} 0.954 & 0.911 & 0.889 \\ 0.046 & 0.089 & 0.074 \\ 1.601 & 0.000 & 0.038 \end{bmatrix}$	$\begin{Bmatrix} p_1(D_1) \\ p_2(D_2) \\ p_3(D_3) \end{Bmatrix} = \begin{Bmatrix} 0.952 \\ 0.048 \\ 0.000 \end{Bmatrix}$
D16	0.1434	$\begin{bmatrix} 0.790 & 0.768 & 0.720 \\ 0.210 & 0.232 & 0.123 \\ 0.000 & 0.000 & 0.158 \end{bmatrix}$	$\begin{Bmatrix} p_1(D_1) \\ p_2(D_2) \\ p_3(D_3) \end{Bmatrix} = \begin{Bmatrix} 0.785 \\ 0.215 \\ 0.000 \end{Bmatrix}$
D17	0.2178	$\begin{bmatrix} 0.701 & 0.689 & 0.567 \\ 0.299 & 0.311 & 0.136 \\ 0.000 & 0.000 & 0.297 \end{bmatrix}$	$\begin{Bmatrix} p_1(D_1) \\ p_2(D_2) \\ p_3(D_3) \end{Bmatrix} = \begin{Bmatrix} 0.697 \\ 0.303 \\ 0.000 \end{Bmatrix}$
D18	0.2210	$\begin{bmatrix} 0.698 & 0.688 & 0.563 \\ 0.302 & 0.312 & 0.136 \\ 0.000 & 0.000 & 0.300 \end{bmatrix}$	$\begin{Bmatrix} p_1(D_1) \\ p_2(D_2) \\ p_3(D_3) \end{Bmatrix} = \begin{Bmatrix} 0.695 \\ 0.305 \\ 0.000 \end{Bmatrix}$
D19	0.4050	$\begin{bmatrix} 0.665 & 0.664 & 0.375 \\ 0.333 & 0.334 & 0.119 \\ 0.002 & 0.002 & 0.506 \end{bmatrix}$	$\begin{Bmatrix} p_1(D_1) \\ p_2(D_2) \\ p_3(D_3) \end{Bmatrix} = \begin{Bmatrix} 0.664 \\ 0.332 \\ 0.004 \end{Bmatrix}$

$$p(R^{(2)}|A_j^{(1)}, A_i^{(2)}, D_d^R) = \sum_{l=1}^{m_R} p(R^{(2)}|R_l^{(1)}, A_j^{(1)}, A_i^{(2)}, D_d^R) p(R_l^{(1)}|D_d^R) \quad (16)$$

$$p(R^{(2)}|D_d^R) = \sum_{j=1}^{m_A} p(R^{(2)}|A_j^{(1)}, A_i^{(2)}, D_d^R) p(A_j^{(1)}|D_d^A) \quad (17)$$

$$p(R^{(2)}|D_d^R) = \sum_{i=1}^{m_R} p(R^{(2)}|(D_d^R)^{(2)}) p(A_i^{(2)}|D_d^A) \quad (18)$$

where  $m_R$  and  $m_A$  are the numbers of intervals in the discretized  $(D_d^R)^{(1)}$  domain and excitation amplitude domain, respectively. The probability of the excitation amplitude of the next cycle being in domain  $D_d^R$  can be computed by

$$p(A_n^{(z)}|D_d^R) = \int_{A_n - \Delta A/2}^{A_n + \Delta A/2} p(A|D_d^A) dA \quad n = 1, 2, \dots, m_A \quad z = 1, 2 \quad (19)$$

Thus, the overall stationary response amplitude probability distribution can be approximated as

$$p(R^{(1)}) = p(R^{(2)}) = \sum_{j=1}^{m_A} p(R^{(1)}|(D_d^R)^{(1)}) p(A_j^{(1)}|D_d^A) \quad (20)$$

### Predictions, Experimental Results, and Simulations

To validate the prediction capability of the semianalytical method, predicted response amplitude PDFs are presented and compared to those obtained from experimental and numerical simulation results. The durations of experiments were sufficiently long to achieve stationarity. However, data were recorded only for short periods of time due to limited storage capacity at the time when the experiment was conducted and the large number of cases examined. Since long duration of simulations are relatively easy to obtain, and may provide better “data sets” for calibrating of the semianalytical method, simulation results were performed for 25,000 excitation cycles to complement experimental results. The experimental tests were conducted with several distinct configurations for the single-degree-of-freedom (SDOF) structural system. In this study, experimental results from Tests D16, D17, and D18 (all subharmonic responses) are selected for comparison with predictions. In these tests, narrow band excitations are used as input to the SDOF system with a 90 deg mooring lines configuration, which exhibit highly nonlinear behavior among several different mooring configurations. Simulated “Tests” D15 and D19 are generated numerically using the Shinozuka [15] formulation in the numerical simulation of narrow band random waves with target variances of Tests D15 and D19 about one-half times that of Test D16 and twice that of Test D18, respectively. These two different target variances are selected to examine the influence of the variance on the accuracy in predicting response amplitude probability. The excitation and system parameter sets are shown in Table 1. Note that  $\rho$  is the autocorrelation of the cosine components of the excitation envelop process with time lag equal to the peak excitation period [14].

The probability of the system response being in one attraction domain through interdomain transitions and corresponding transition probability matrix  $K$  are listed in Table 2. Subscripts 1, 2, and 3 represent small harmonic domain, 1/2 subharmonic domain, and large harmonic domain, respectively. Observe that when the excitation intensity, i.e., variance, increases, the excitation amplitudes become large and the excitation amplitude probability distribution is shifted to the right. As the excitation amplitude increases from Tests D15 to D19, the probability that the system

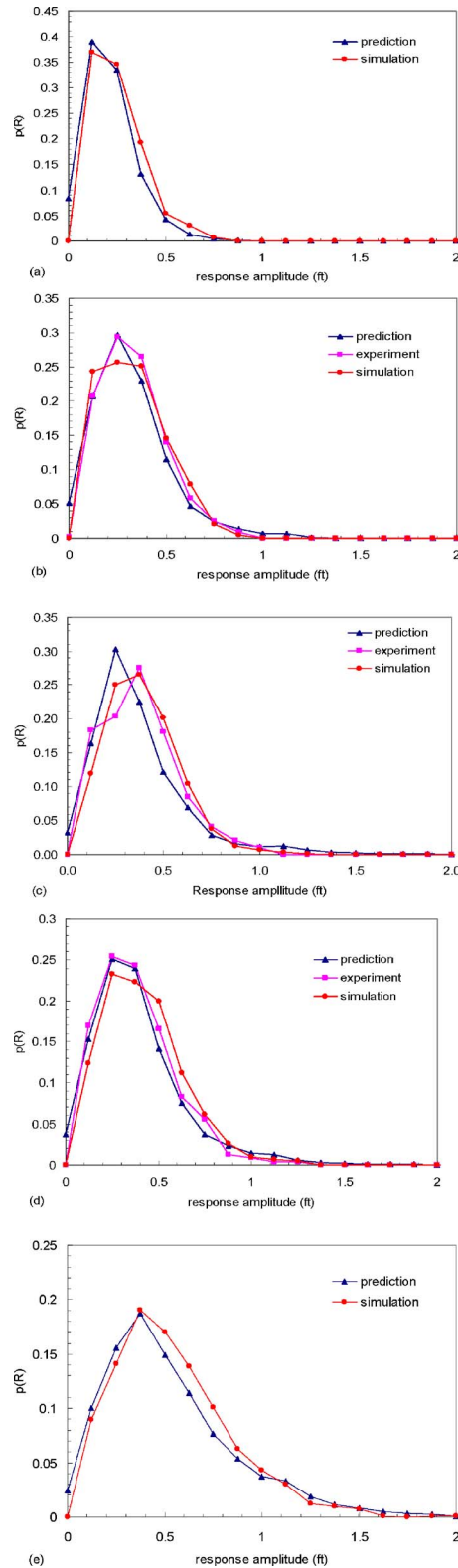


**Fig. 7 Overall response amplitude distribution: (a) Test D15; (b) Test D16; (c) Test D17; (d) Test D18; (e) Test D19**

response staying in the small amplitude domain decreases. Thus, the value of  $p(1|1)$  in the transition matrix  $K$  decreases while both  $p(2|2)$  and  $p(3|3)$  increases.

The overall response amplitude PDFs obtained by Eq. (20), numerical simulation results, and experimental results are pre-

sented in Fig. 7 for the five cases examined. It can be observed that, in each case, the prediction obtained from the analytical procedure accurately matches both the experimental and simulation results.

### Concluding Remarks

Three co-existing attraction domains, i.e., small amplitude harmonic,  $1/2$  subharmonic, and large amplitude harmonic attraction domains, are identified for the NSND model with system coefficients obtained by applying reverse multiple-input/single-output technique. However, according to the interdomain transition probabilities, it is observed that the steady-state probability of response amplitude being in the large harmonic attraction domain is sufficiently small to be neglected for the excitations of Tests D16, D17, and D18. Thus, the contribution to the overall response amplitude distribution from the intradomain transition probability of large harmonic attraction domain is also neglected.

The predicted response amplitude distributions are compared with both experimental result and numerical simulation in Fig. 7. It is observed that the semianalytical method predicted the response amplitude distribution accurately. The shape of distribution, the location of peak, and maximum probability of response amplitude are in good agreement with experimental results. These results validate the ability of semianalytical method in predicting nonlinear system response under narrow band excitation.

The response amplitude probability distribution can be obtained from the analytical procedure when the stochastic property of excitation amplitude is specified. The predicted results for the wide range of excitation parameters can be readily used in structural design, control, and other applications without simulations.

### Acknowledgment

Partial financial support from the U.S. Office of Naval Research (Grant Nos. N00014-04-10008 and N00014-06-10326) is gratefully acknowledged.

### References

- [1] Bernitsas, M. M., and Kokkinis, T., 1984, "Global Static Instability of Risers," *J. Ship Res.*, **28**(4), pp. 261–271.
- [2] Papoulias, F. A., and Bernitsas, M. M., 1988, "Autonomous Oscillations, Bifurcations and Chaotic Response of Moored Vessels," *J. Ship Res.*, **32**(3), pp. 220–228.
- [3] Gottlieb, O., and Yim, S. C., 1992, "Nonlinear Oscillations, Bifurcations and Chaos in a Multi-Point Mooring System With a Geometric Nonlinearity," *Appl. Ocean. Res.*, **14**(6), pp. 241–257.
- [4] Gottlieb, O., and Yim, S. C., 1993, "Drag-Induced Instability and Chaos in Mooring Systems," *Ocean Eng.*, **129**(6), pp. 569–599.
- [5] Garza-Rios, L. O., and Bernitsas, M. M., 1996, "Analytical Expressions of the Stability & Bifurcation Boundaries for General Spread Mooring Systems," *J. Ship Res.*, **40**(4), pp. 337–350.
- [6] Thompson, J. M. T., and Stewart, H. B., 1986, *Nonlinear Dynamics and Chaos*, 1st ed., Wiley, New York; 2002, *ibid.*, 2nd ed., Wiley, New York.
- [7] Nayfeh, A. H., and Mook, D. T., 1979, *Nonlinear Oscillations*, Wiley, New York.
- [8] Lin, H., and Yim, S. C. S., 1995, "Noisy Nonlinear Motions of Moored Systems. Part I: Analysis and Simulation," *J. Waterway, Harb. and Coast. Engrg. Div.*, **123**(5), pp. 287–295.
- [9] Yim, S. C., and Lin, H., 2000, "Noisy Nonlinear Motions of a Moored System, II: An Experimental Study," *J. Waterway, Port, Coastal, Ocean Eng.*, **128**(3), pp. 113–120.
- [10] Narayanan, S., and Yim, S. C., 2004, "Modeling and Identification of a Nonlinear SDOF Moored Structure, Part I, Analytical Models and Identification Algorithms," *ASME J. Offshore Mech. Arct. Eng.*, **126**(2), pp. 175–182.
- [11] Yim, S. C., and Narayanan, S., 2004, "Modeling and Identification of a Nonlinear SDOF Moored Structure, Part II, Results and Sensitivity Study," *ASME J. Offshore Mech. Arct. Eng.*, **126**(2), pp. 183–190.
- [12] Yim, S. C., Myrum, M. A., Gottlieb, O., Lin, H., and Shih, I., 1993, "Summary and Preliminary Analysis of Nonlinear Oscillations in a Submerged Mooring System Experiment," *Ocean Engineering Program, Oregon State University*, Report No OE-93-03.
- [13] Chakrabarti, S. K., 2002, *The Theory and Practice of Hydrodynamics and Vibration*, World Scientific, New Jersey.
- [14] Ochi, M. K., 1990, *Applied Probability and Stochastic Processes in Engineering and Physical Sciences*, Wiley, New York.
- [15] Shinozuka, M., 1971, "Simulation of Multivariate and Multidimensional Random Processes," *J. Acoust. Soc. Am.*, **49**, pp. 357–367.